INTERNATIONAL JOURNAL FOR NUMERICAL METHODS IN FLUIDS
Int. J. Numer. Meth. Fluids **28**: 215–224 (1998)

ORTHOGONAL GRID GENERATION FOR NAVIER–STOKES COMPUTATIONS

MANOJ T. NAIR AND T.K. SENGUPTA*

Department of Aerospace Engineering, Indian Institute of Technology, Kanpur 208 016, India

SUMMARY

Body conforming orthogonal grids were generated using a fast hyperbolic method for aerofoils, and were used to solve the Navier–Stokes equation in the generalized orthogonal system for the first time for time accurate simulation of incompressible flow. For grid generation, the Beltrami equation and the definition equation for the orthogonality are solved using a finite difference method. The grids generated around aerofoils by this method have better orthogonality than the results published by earlier investigators. The Navier–Stokes equation at Reynolds numbers of 3000 and 35000 for NACA 0012 and NACA 0015 respectively, have been solved as an application. The obtained results match quite well with the corresponding experimental results. © 1998 John Wiley & Sons, Ltd.

KEY WORDS: orthogonal grids; hyperbolic grid generation; Navier–Stokes equations; higher-order methods

1. INTRODUCTION

One of the primary activities in computational fluid dynamics is obtaining a suitable grid for the solution of the governing differential equation. In the present study, our concern is with orthogonal structured grid generation in two dimensions. The literature in the area of structured grid generation is extensive and some of the major efforts are given by Fletcher [1], Thompson *et al.* [2] and Eiseman [3]. Any effective grid generation strategy requires

1. good control over grid spacing to resolve all the relevant length scale of the physical problem, and
2. lower numerical error associated with grid generation with little computational effort.

Orthogonal grids may be preferred for the following reasons:

1. simpler transformed equations and their differenced form,
2. accurate and easy implementation of boundary conditions,
3. smaller numerical errors of the solution for governing differential equations by faster methods. The accuracy and speed of methods could be due to the mapping, as seen in the present case.

Orthogonal grids is the optimum choice between complete non-orthogonal grids and conformal mapping. Orthogonal grids have been produced by solving either elliptic partial differential equations [4–6] or hyperbolic differential equations [7,9–11].

* Correspondence to: Department of Aerospace Engineering, Indian Institute of Technology, Kanpur 208 016, India.

CCC 0271–2091/98/120215–10$17.50

Received August 1996
Revised February 1997

Ryskin and Leal [4], Duraiswami and Prosperetti [5] and Eca [6] have solved the covariant Laplace equations,

$$\frac{\partial}{\partial\xi}\left(f\frac{\partial x}{\partial\xi}\right)+\frac{\partial}{\partial\eta}\left(\frac{1}{f}\frac{\partial x}{\partial\eta}\right)=0, \qquad \frac{\partial}{\partial\xi}\left(f\frac{\partial y}{\partial\xi}\right)+\frac{\partial}{\partial\eta}\left(\frac{1}{f}\frac{\partial y}{\partial\eta}\right)=0, \tag{1}$$

for transformation from the physical (x, y) plane to the mapped (ξ, η) plane. In the above equation, f is the distortion function, given by

$$f=\frac{h_{22}}{h_{11}}=\frac{\sqrt{x_\eta^2+y_\eta^2}}{\sqrt{x_\xi^2+y_\xi^2}}. \tag{2}$$

In Ryskin and Leal [4], f distribution was interpolated as a bivariate distribution; Duraiswami and Prosperetti [5] used a specific method of obtaining a class of f functions, where it is expressed as a product of two independent functions of the transformed co-ordinates with conditions imposed on them for proper grid generation. However, a general distortion function (as used here) according to these authors is *highly desirable to achieve a more localized control on the density of co-ordinate lines*. For the specific class of f, the generated grids in Reference [5] for aerofoils have better orthogonal property than other cited references—excepting the present results. Eca [6] used a procedure to iteratively obtain f along with the main grid generation iteration for the resultant non-linear system, a procedure that was used earlier in Reference [8]. The disadvantage of the methods used by Ryskin and Leal [5] and the *strong constraint method* of Duraiswami and Prosperetti [4] is that the grid point distribution on the defining boundaries is made to change as part of the iterative method. In the *weak constraint method* [4,6,8] the grids are generated with fixed boundary points. Note that the Equation (1) is obtained by utilising the definition of the distortion function (Equation (2)) and the orthogonality constraint

$$g_{12}=x_\xi x_\eta+y_\xi y_\eta=0. \tag{3}$$

It has been pointed out in References [5,8] that any solution of Equation (1) alone does not necessarily satisfy the orthogonality condition given by Equation (3).

The hyperbolic methods in this context are superior in producing orthogonal grids because they use Equation (3) as one of the governing grid generation differential equations. In general, hyperbolic methods are attractive for external flow problems where the shape of the outer boundary is not a constraint. However, they have also been successfully implemented for internal flow problems [10,11] by relaxing orthogonality.

In the present method, Equation (3) along with one of the Beltrami equations as given in Equation (7) in the next section (referred to as generalized Cauchy–Riemann equation in Reference [4]) are solved with the arc length in the normal direction prescribed. This method of using constant arc length is similar to the suggestion of Dwyer [12], to overcome the problem of grid shock formation in hyperbolic grid generation over strong concave surfaces. In Reference [9] the finite difference method was compared with a spectral method of solving the Beltrami equation, and was found to be superior with better orthogonal properties.

The essential ideas for grid generation are given in the next section. In Section 3, the results and discussion are presented for the grid generation procedure. The produced grids have been used for solving the two-dimensional incompressible unsteady Navier–Stokes equation and the computational results are compared with experimental results.

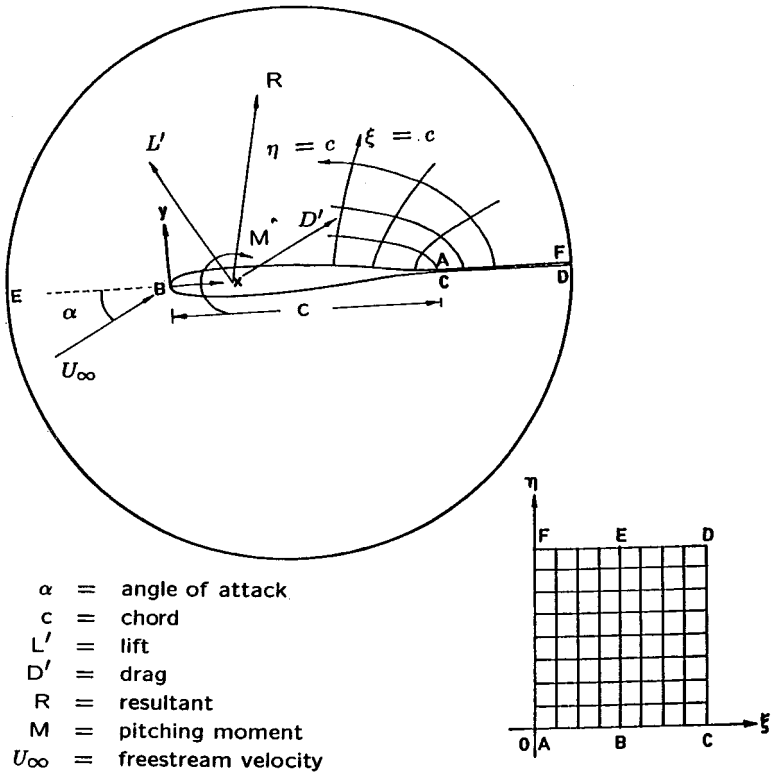

Figure 1. The physical and computational domains for the O-type grid.

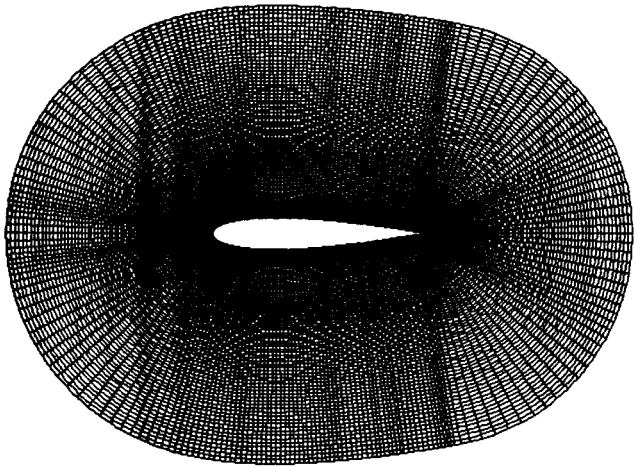

Figure 2. Grid generated around NACA 0015 aerofoil. Only the first 101 η-lines are shown. There are 233 points on the aerofoil surface.

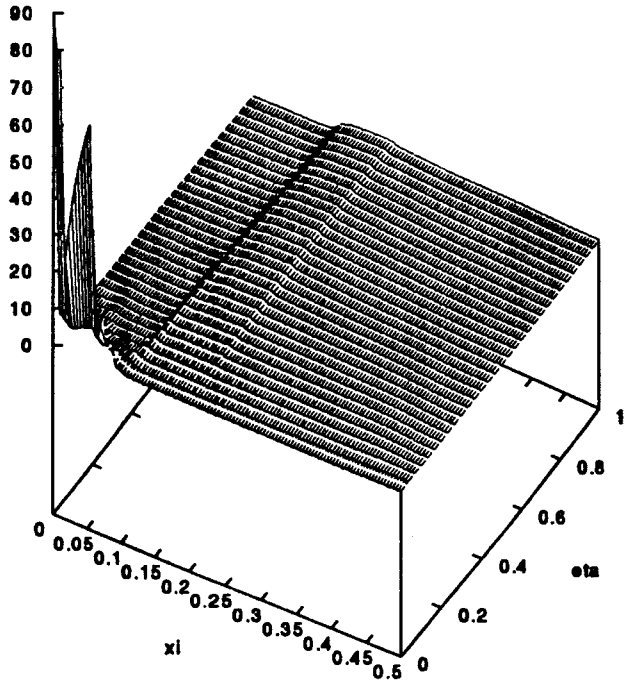

Figure 3. The f distribution in the (ξ, η) plane. Note the strong dependence of f on (ξ, η) near the trailing edge only.

2. FORMULATION

The general mapping in two dimensions is given by

$$\xi = \xi(x, y), \qquad \eta = \eta(x, y). \tag{4}$$

The metrics of the transformation is given by

$$g = \begin{vmatrix} g_{11} & g_{12} \\ g_{21} & g_{22} \end{vmatrix}, \tag{5}$$

where

$$g_{ij} = \sum_{k=1}^{2} \frac{\partial x^k}{\partial \xi^i} \frac{\partial x^k}{\partial \xi^j}.$$

The scale factors of the transformation are given by

$$h_{ij} = \sqrt{g_{ij}}. \tag{6}$$

The orthogonality condition given by Equation (3) can be combined with the definition of the Jacobian to yield the Beltrami equation

$$x_\eta = f y_\xi, \qquad y_\eta = -f x_\xi. \tag{7}$$

It is easy to see that Equation (1) follows straight from Equation (7) upon eliminating x and y, respectively.

In the present exercise O-type grids are produced using the finite difference method. Here, Equation (3) and either part of Equation (7) are solved along with the prescribed arc length in the hyperbolic direction by taking the following steps:

1. The points on the body are distributed along $\eta = 0$ line which fixes the scale factor h_{11} distribution on this line.
2. The grid line increment ΔS_η in the η-direction is prescribed and this fixes the other scale factor h_{22}, given by

$$h_{22} = \frac{\Delta S_\eta}{\Delta \eta}. \tag{8}$$

   Thus, the distortion function f can be evaluated on $\eta = 0$ line.
3. Equation (3) and either part of Equation (7) are then integrated by one step. This produces (x, y) co-ordinates of the $\eta = \Delta\eta$ line.
4. Steps (1)–(3) are repeated to obtain the grid lines.

The present procedure for the evaluation of f not only makes the grid generation process very fast, it also gives a rational basis for the choice of the function f. Unlike previous studies [6,8], this process of fixing the distortion function makes the governing grid generation equations linear and hence the grid generation process is very fast. Furthermore, the ability to prescribe the grid line spacing in the normal direction is a very useful feature of the generated grids for viscous flow calculations.

3. RESULTS AND DISCUSSION

The above mentioned method has been implemented on various aerofoils. In Figure 1 the physical and computational plane are illustrated. For a typical O-type grid the physical body is represented as ABC, where the cuts AF and CD are introduced starting from the trailing edge so that the computational domain is connected simply. Dirichlet conditions are prescribed

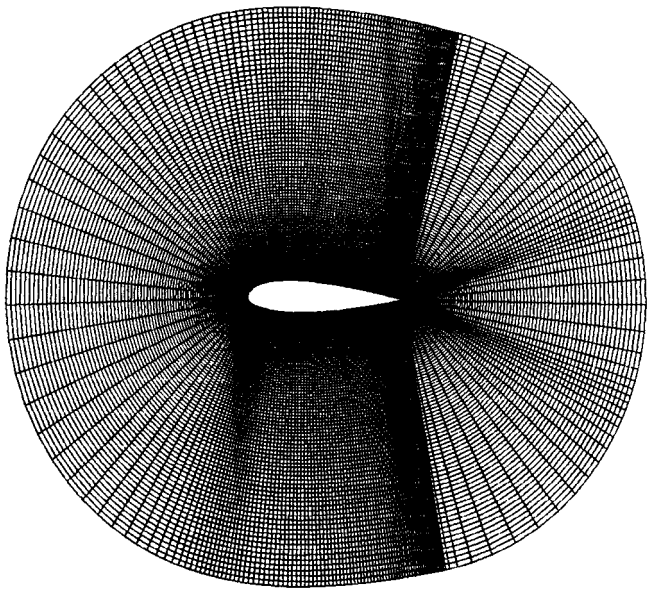

Figure 4. Grid generated around NACA 23018 aerofoil. Only the first 101 η-lines are shown. There are 229 points on the aerofoil surface.

i) Experimental visualization

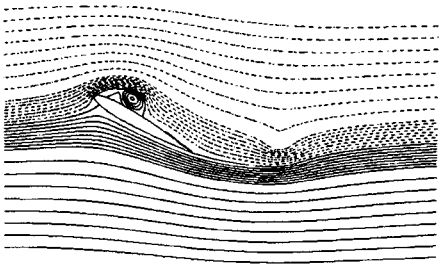

ii) computed streamlines

(a) iii) Computed vorticity contours.

Figure 5. (a) Comparison between experimental (Reference [13], also M. Coutanceau, private communication) and computational results at $t = 1.0$ for NACA 0012 at $Re = 3000$ and $\alpha = 30°$. The computations are done on a 233×301 grid. (b) Comparison between experimental (Reference [13], also M. Coutanceau, private communication) and computational results at $t = 2.25$ for NACA 0012 at $Re = 3000$ and $\alpha = 30°$. The computations are done on a 233×301 grid. (c) Comparison between experimental (Reference [13], also M. Coutanceau, private communication) and computational results at $t = 3.25$ for NACA 0012 at $Re = 3000$ and $\alpha = 30°$. The computations are done on a 233×301 grid.

on ABC and the grid spacing in the wake of the aerofoil is achieved by distributing points on the cuts AD and CF. The first grid line is located as close as 0.00001 chord of the aerofoil. The successive grid lines are expanded smoothly by increasing the spacing by a constant value.

The first 100 lines in the hyperbolic direction of the grid generated for NACA 0015 are shown in Figure 2. The slope discontinuity at the trailing edge is avoided by fitting a parabola in the open trailing edge, with continuous slope everywhere. There are 233 points in the ξ-direction, 301 lines in the η-direction, and the outer boundary is 14.76 chords away. The included angle between the constant ξ- and η-lines are virtually orthogonal everywhere except at three points along the second η-line, where the worst departure from the orthogonality is given by the included angle of 89.476°. The included angle is calculated from

$$\theta = \cos^{-1}\left[\frac{g_{12}}{h_{11}h_{22}}\right]. \tag{9}$$

In calculating the metrics, second-order central differences are used wherever possible. The major advantage of the present method is that the addition and deletion of points only have local effects. The orthogonality property of the generated grid is better than the earlier efforts [7,5,6]. For a cambered turbine blade, Steger and Chaussee [7] have reported the worst non-orthogonality as $\approx 20\%$; Duraiswami and Prosperetti [5] reported 1.11° as the maximum departure from orthogonality and Eca [6] reports this as 4.41° for the NACA 0015 aerofoil. It is clear that these grids cannot be used as they are to solve the Navier–Stokes equation written in the orthogonal co-ordinate system. In Figure 3 the distortion function has been plotted as a function of η and ξ for NACA 0012. This figure shows that the present method uses f, which is quite different than the analytic expression used in Reference [5]. In fact, the local control of grid lines as seen in the present method precludes such simple representation of f. Although f depends strongly on ξ and η near the trailing edge, later on it is a weak function of η.

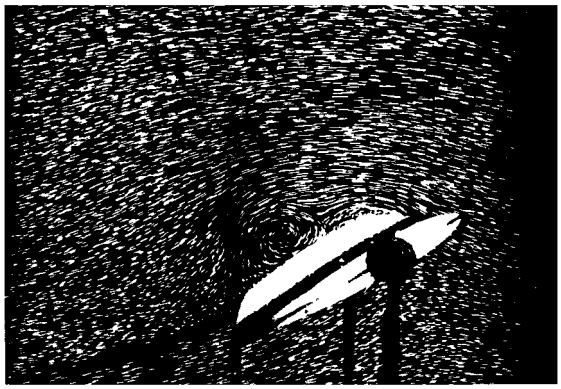

i) Experimental visualization

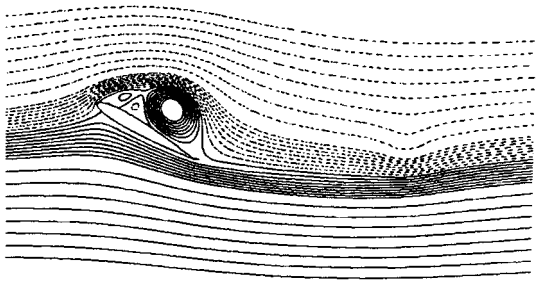

ii) computed streamlines

(b) iii) Computed vorticity contours.

Figure 5 (*Continued*)

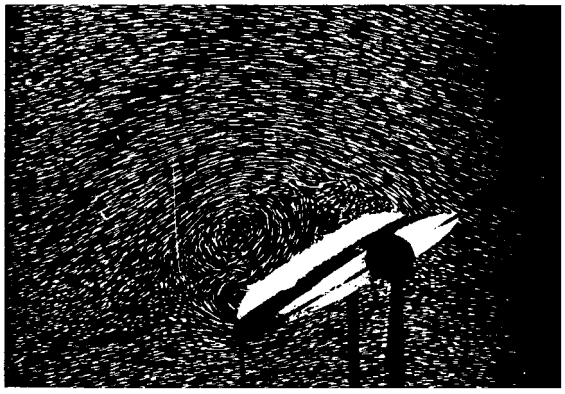

i) Experimental visualization

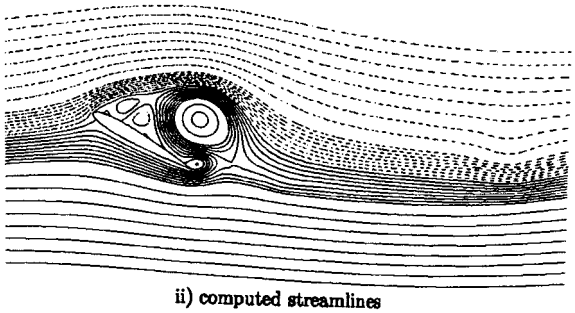

ii) computed streamlines

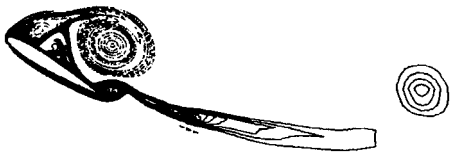

(c) iii) Computed vorticity contours.

Figure 5 (*Continued*)

The grid for a thicker (18%) aerofoil with camber (NACA 23018) is shown in Figure 4. The first 101 η-lines of the generated grids of size (229×301) are shown and the effect of the large camber on generated grids produces grid clustering on the lower side near leading edge, due to the shape of the camber line. The worst non-orthogonality here is obtained near the trailing edge with a value of $\theta = 89.33°$. Once again, the open trailing is closed by an analytic curve affecting only the last 0.01% of the chord near the trailing edge.

The grid generated around NACA 0015 has also been used in computing the Navier–Stokes equation. In this case, the worst non-orthogonality is given by $\theta = 89.526°$. This value is the best in comparison with published results. In Reference [5] this value has been reported as $\theta = 88.89°$, while Reference [6] gives a value of $\theta = 85.59°$.

To show the application of the grids generated, they were used to investigate the flow field past an impulsively started NACA 0012 aerofoil at $Re = 3000$ and at an angle of attack of 30°, and NACA 0015 aerofoil at $Re = 35000$ and at an angle of attack of 30°. The Reynolds number is based on the chord of the aerofoil and the free-stream speed. The present objective

is to show the effectiveness of the grid generation technique, therefore the results presented here are for the early times where computed results are compared with sequence of flow streamlines as obtained experimentally by Ohmi *et al.* [13] and Morikawa and Gronig [14]. The additional figures included for the case of $Re = 3000$ and $\alpha = 30°$ were provided by Coutanceau (private communication).

The effectiveness of the grid generation method is shown by solving the Navier–Stokes equation in streamfunction–vorticity formulation. The streamfunction–vorticity equation is solved for the orthogonal grids and is given by

$$\frac{\partial}{\partial \xi}\left(\frac{h_{22}}{h_{11}}\frac{\partial \psi}{\partial \xi}\right)+\frac{\partial}{\partial \eta}\left(\frac{h_{11}}{h_{22}}\frac{\partial \psi}{\partial \eta}\right)= -h_{11}h_{22}\omega, \tag{10}$$

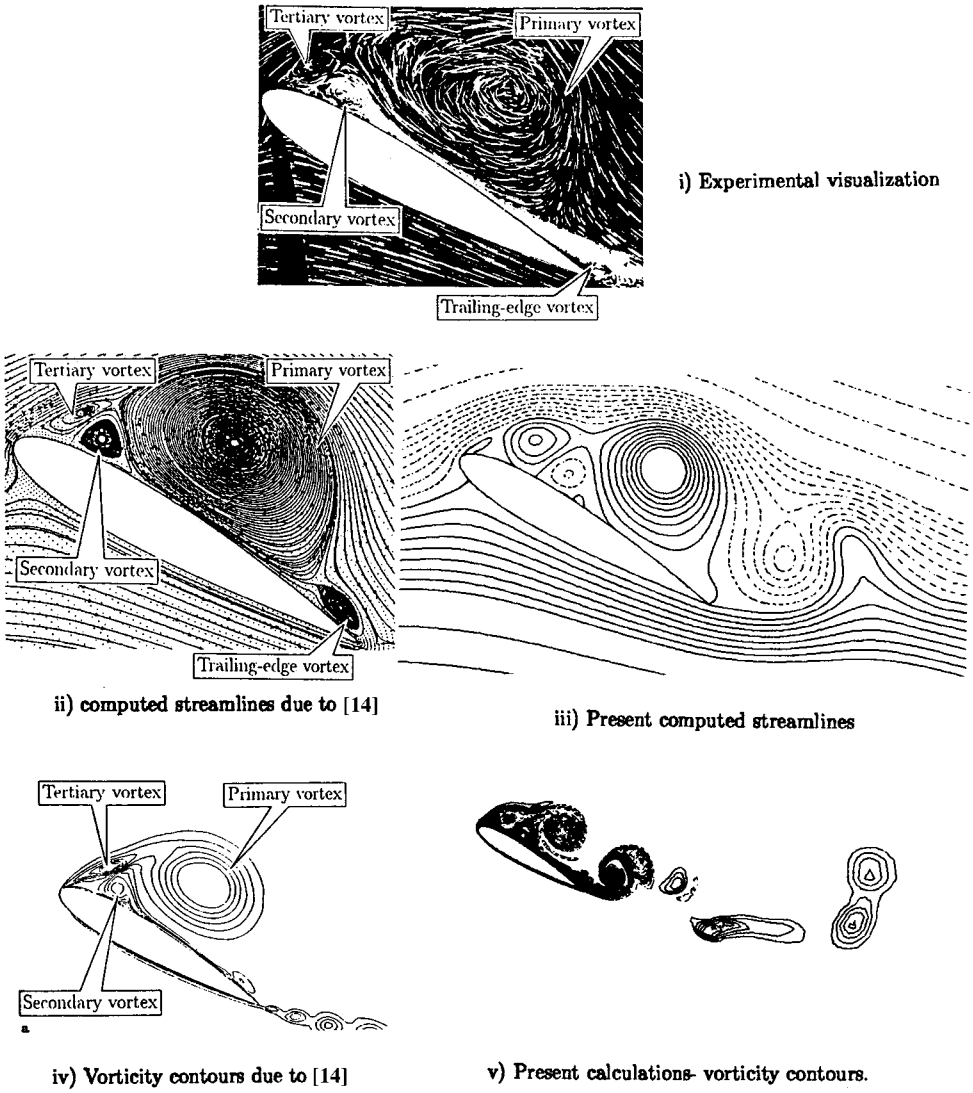

Figure 6. Comparison between experimental [14] and computational results at $t = 2.9037$ for NACA 0015 at $Re = 35000$ and $\alpha = 30°$. The computations are done on a 233×301 grid.

and

$$h_{11}h_{22}\frac{\partial\omega}{\partial t}+h_{22}u\frac{\partial\omega}{\partial\xi}+h_{11}v\frac{\partial\omega}{\partial\eta}=\frac{1}{Re}\left\{\frac{\partial}{\partial\xi}\left(\frac{h_{22}}{h_{11}}\frac{\partial\omega}{\partial\xi}\right)+\frac{\partial}{\partial\eta}\left(\frac{h_{11}}{h_{22}}\frac{\partial\omega}{\partial\eta}\right)\right\}. \tag{11}$$

For the results shown in Figure 5(a–c) up to $t = 3.25$, a third-order upwind scheme was used for the convective terms of the vorticity transport equations (11). The diffusion terms are discretized using second-order central differencing.

The plots show that the computed results match quite well with the experimental results showing the large vortical structures. The present method of solving the Navier–Stokes equation is accurate due to the higher-order upwinding method used.

Next, some results for the NACA 0015 aerofoil at $Re = 35000$ are shown, for which Morikawa and Gronig [14] have given some experimental and computational results. The aerofoil in the tunnel was started with constant initial acceleration up to a non-dimensional time of 0.598, compared with the case of Ohmi *et al*. [13], where the experiment was started almost impulsively. The experimental arrangement for Ohmi *et al*. [13] gives this start-up non-dimensional time at around 0.1, depending on the size of the model. The detailed comparison of results for the impulsive start and accelerated start will be reported elsewhere. Only the result in Figure 6 for the impulsively started NACA 0015 aerofoil at $Re = 35000$ at $\alpha = 30°$ is shown here.

REFERENCES

1. C.A.J. Fletcher, *Computational Techniques in Fluid Dynamics*, Vol. I and II, Springer, New York, 1987.
2. J.F. Thompson, Z.U.A. Warsi and C.W.J. Mastin, *J. Comput. Phys*., **47**, 1 (1982).
3. P.R. Eiseman, 'Grid generation for fluid mechanics computation', *Ann. Rev. Fluid Mech*., **17**, 487–522 (1985).
4. G. Ryskin and L.G. Leal, 'Orthogonal mapping', *J. Comput. Phys*., **50**, 71–100 (1983).
5. R. Duraiswami and A. Prosperetti, 'Orthogonal mapping in two dimensions', *J. Comput. Phys*., **98**, 254–268 (1982).
6. L. Eca, '2D orthogonal grid generation with boundary point distribution control', *J. Comput. Phys*., **125**, 440–453 (1996).
7. J.L. Steger and D.S. Chaussee, 'Generation of body-fitted coordinates using hyperbolic partial differential equations', *Siam J. Sci. Stat. Comput*., **1**, 431–437 (1980).
8. S. Sengupta and T.K. Sengupta, 'Orthogonal body-fitted grid generation in two dimensions—some theoretical problems and solutions', *Proc. 5th Int. Conf. on Numerical Methods in Laminar and Turbulent Flows*, Montreal, Canada, 1987.
9. M.T. Nair and T.K. Sengupta, 'An accurate method for orthogonal grid generation in two dimensions', C. Taylor and P. Durbetaki (eds.), *Proc. 9th Int. Conf. in Numerical Methods for Laminar and Turbulent Flows*, Pineridge Press, Swansea, UK, 1995.
10. Y.N. Jeng, Y.L. Shu and W.W. Lin, 'Grid generation for internal flow problem by methods using hyperbolic equations', *Numer. Heat Trans. B*, **27**, 43–61 (1995).
11. J.Q. Cordova and T.J. Barth, 'Grid generation for general two-dimensional regions using hyperbolic equation', AIAA 26th Aerospace Sciences Meeting, Reno Nevada, *Paper No. AIAA-88-0520*, 1988.
12. H.A. Dwyer, 'A geometric interpretation of hyperbolic grid generation', *Comput. Fluids*, **23**, 737–748 (1994).
13. K. Ohmi, M. Coutanceau, O. Daube and L. Ta Phuoc, 'Further experiments on vortex formation around an oscillating and translating airfoil at large incidences', *J.F.M*., **225**, 607–630 (1991).
14. K. Morikawa and H. Gronig, 'Formation and structure of vortex systems around a translating and oscillating airfoil', Z. *Flugwiss. Weltraumforsch*., **19**, 391–396 (1995).

